2020 IEEE/ASME International Conference on
Advanced Intelligent Mechatronics (AIM), Boston, USA
(Virtual Conference), July 6-9, 2020

Assist-As-Needed Control of a Wearable Lightweight Knee Robotic Device

Kyle Hunte, Siyu Chen, Jingang Yi, and Hao Su

Abstract— **Knee joint actuation plays a critical role to keep human walking locomotion and balance under abnormal conditions, such as foot slip or work-related musculoskeletal disorders etc. Wearable assistive robotic knee devices provide additional support and actuation for human walkers. We present assist-as-needed control strategy for a lightweight, highly-backdrivable soft knee assistive device. The control design takes advantages of the custom-built high-performance knee assistive device and the muscle synergy-based human walking actuation model. A model predictive control (MPC) design is used for real-time tuning physical human-robot interactions. Human-in-the-loop simulation results are presented to demonstrate the performance of the robotic control systems under normal walking condition.**

I. Introduction

Knee joint actuation plays a critical role in human locomotion and balance under abnormal conditions, such as foot slip [1], [2] or work-related musculoskeletal disorders [3] etc. Wearable assistive robotic knee devices provide additional support and actuation for human walkers [4], [5]. Predicting human performance, dynamic variations and noise are a few of the challenges encountered when developing real-time controllers. The goal of this work is to develop an assist-as-needed control of wearable knee robotic device.

Various control strategies have been proposed for control of wearable assistive robotic devices [6]–[8]. Combining impedance control with series elastic actuators (SEA) or similar robotic mechanisms, e.g., [9], [10] is common. In these designs, specified torque profiles are used as the tracking targets and the human applied torques is obtained by measurements (e.g., electromyography (EMG) sensors used in [11], [12]). Optimization is another design approach (e.g., [4], [13]). However optimization is only effective for regularly periodic human motion at steady-state walking locomotion. Therefore it is difficult to use in the design of a controller for perturbed gait profiles such as foot slip or trip.

For everyday usage, wearable assistive devices are required to be light-weight, highly-backdrivable with a large-bandwidth for quick responses. The design of wearable knee and hip assistive devices in [14], [15] use the custom-built drive motor to satisfy the previously mentioned requirements. Instead of using SEA mechanisms like many exoskeletons or wearable assistive devices (e.g., [9], [10]), quasi-direct drive (QDD) actuation is used to achieve the desired performance without need of high-ratio gearbox. The desired torque profiles in the preliminary testings are obtained by simply interpolating human walking profiles in [16]. A similar design is demonstrated in other high-performance legged robotics [17]. We use the prototype model in [15] for the human-in-the-loop study in this work.

To predict the human reaction under normal or perturbed walking conditions without using EMG or other muscle activity sensors, we consider the muscle synergy model-based joint torque estimation. Muscle synergy represents a group of relationship-fixed muscle activities during human motion and the muscle synergies for normal walking and foot slip are presented in [18] and [19], respectively. In [20], [21], the muscle synergy model is used to predict the upper-limb strength capacity without using the muscle activation sensors such as EMG. We take the advantages of these developments and estimate the knee joint torques under normal walking conditions and incorporate them into the wearable assistive device control.

In this paper, we present an assist-as-needed control strategy for a lightweight, highly-backdrivable knee assistive device. The control design is built on the dynamics model for the QDD device and a muscle synergy-based human actuation prediction. A model predictive control (MPC) is designed to integrate the human actuation prediction and the QDD device to achieve the desired human-robot interactions properties. We implement and simulate the design using OpenSim environment [22] with motion and force data from human walking experiments. The human-in-the-loop (HIL) simulation results demonstrate the control design performance. The main contribution of the work lies in the MPC assist-as-needed control of wearable knee robotic device with human joint torque estimation without need of real-time muscle activation measurements. Integrated with the lightweight, highly-backdrivable, high-bandwidth device design, the proposed control system provides an enabling tool for potential implementation for wearable assistive devices in personal daily activities.

II. Muscle Synergy Models for Human Walking and QDD Assistive Device

A. Muscle Synergy Model-based Torque Estimation

Muscle synergy represents a group of muscles that act together at a fixed activation ratio among them. Considering

The work was supported in part by the US National Science Foundation under award CMMI-1762556.

K. Hunte is with the Department of Electrical and Computer Engineering, Rutgers University, Piscataway, NJ 08854 USA (email: kdh95@scarletmail.rutgers.edu).

S. Chen and J. Yi are with the Department of Mechanical and Aerospace Engineering, Rutgers University, Piscataway, NJ 08854 USA (e-mail: siyu.chen@rutgers.edu; jgyi@rutgers.edu).

H. Su is with the Department of Mechanical Engineering, The City University of New York, New York, NY 10023 USA (e-mail: hao.su@ccny.cuny.edu).

Authorized licensed use limited to: City College of New York. Downloaded on May 21,2021 at 18:47:40 UTC from IEEE Xplore. Restrictions apply.

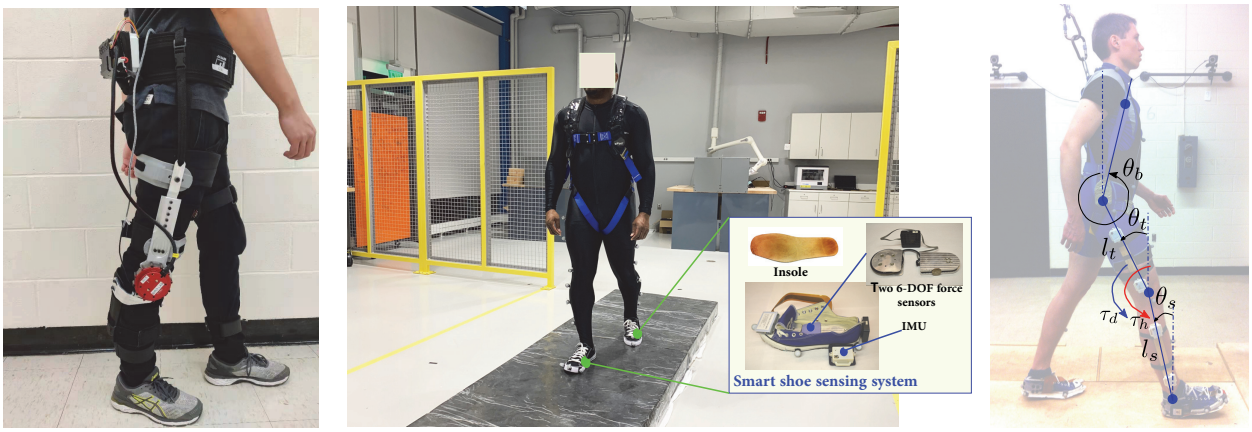

(a) (b) (c)

Fig. 1. (a) The light-weight, highly-backdrivable wearable knee assistive device developed by City University of New York (CUNY) [14]. (b) The slip and fall experimental setup with various sensor suites. (c) Schematic of the wearable device with human lower-limb during walking gait.

the joint angle vector $\boldsymbol{q}_h$, muscle activation is expressed as the summation of spatial and temporal patterns of muscle synergies as

$$\boldsymbol{M}(\boldsymbol{q}_h, t) = \sum_{i=1}^{n} c_i(t)\boldsymbol{w}_i = \boldsymbol{W}(\boldsymbol{q}_h)\boldsymbol{C}(t), \tag{1}$$

where $\boldsymbol{M}(\boldsymbol{q}_h, t) \in \mathbb{R}^N$ is the muscle activation vector, N is the number of muscles, matrix $\boldsymbol{W}(\boldsymbol{q}_h) = [\boldsymbol{w}_1 \cdots \boldsymbol{w}_n] \in \mathbb{R}^{N\times n}$ represents n muscle synergies, and activation level $\boldsymbol{C}^T(t) = [c_1(t) \cdots c_n(t)]^T \in \mathbb{R}^n$. The applied human knee torque τ_h (as shown in Fig. 1(c)) can be written as

$$\tau_h(\boldsymbol{q}_h, \dot{\boldsymbol{q}}_h) = \boldsymbol{A}_F(\boldsymbol{q}_h, \dot{\boldsymbol{q}}_h)\boldsymbol{C}(t), \tag{2}$$

where $\boldsymbol{A}_F(\boldsymbol{q}_h, \dot{\boldsymbol{q}}_h) \in \mathbb{R}^{1\times n}$ is the gain matrix and each column of $\boldsymbol{A}_F$ is a base force vector for synergy direction.

To estimate the joint torque τ_h by using (2), we obtain the predicted values of $\boldsymbol{A}_F(\boldsymbol{q}_h, \dot{\boldsymbol{q}}_h)$ offline and $\boldsymbol{C}(t)$ in real-time. Using ground reaction forces (GRF) and measurements from EMG sensors, we obtain an estimate of $\boldsymbol{A}_F(\boldsymbol{q}_h, \dot{\boldsymbol{q}}_h)$ off-line using the method of least-squares. The real-time prediction of $\boldsymbol{C}(t)$ is obtained by training a neural network. We consider $\boldsymbol{C}(t) = \boldsymbol{C}(\Delta\boldsymbol{q}_h, \Delta\dot{\boldsymbol{q}}_h, \Delta\ddot{\boldsymbol{q}}_h)$, where $\Delta\boldsymbol{q}_h(t) = \boldsymbol{q_h}(t) - \boldsymbol{q}_h^d(t)$ and $\boldsymbol{q}_h^d(t)$ is the human normal gait profile. For a neural network to estimate $\boldsymbol{C}(t)$, a radial basis function is used to obtain the predictions as $\boldsymbol{C}(\boldsymbol{W}, \boldsymbol{\nu}) = \boldsymbol{W}^T\boldsymbol{S}(\boldsymbol{\nu})$, where $\boldsymbol{S}(\boldsymbol{\nu}) = \{s_i(\boldsymbol{\nu})\}$, $s_i(\boldsymbol{\nu}) = \exp\left[\frac{-(\boldsymbol{\nu}-\boldsymbol{\mu}_i)^T(\boldsymbol{\nu}-\boldsymbol{\mu}_i)}{\eta_i^2}\right]$, $i = 1, \ldots, p$, is the base function and p is the total number of base functions. Parameters $\boldsymbol{\nu}$ and $\boldsymbol{W}$ are the network input and weight vector, respectively, and $\boldsymbol{\mu}_k$ and η_k are constants. We use $\boldsymbol{\nu}_C = [\Delta\boldsymbol{q_h}\ \Delta\dot{\boldsymbol{q}}_h\ \Delta\ddot{\boldsymbol{q}}_h]^T$.

In this work a total of eight muscle activities are measured by the EMG sensors, including rectus femoris (RFEM), vastus medialis (VMED), vastus lateralis (VLAT), semitendinosus (SEMT), biceps femoris long head (BFLH), lateral gastrocnemius (LGAS), medial gastrocnemius (MGAS), and tibialis anterior (TA). The synergy activation and EMG data process are reconstructed through non-negative factorization (NNMF) method.

B. QDD Wearable Assistive Device

Fig. 3 presents the dynamic model of the assistive device (as shown in Fig. 1(a)) coupled with the human lower limb. Similar to [15], the model consists of three parts: the electromechanical module, torque transmission and human-device interface modules. The electromechanical module includes a DC motor and the torque transmission is a gearbox unit connected to the motor.

For the electromechanical system, we denote the input voltage, current and generated torque as V_c, i, and τ_m, respectively and the dynamic model is given as

$$V_c - k_b\dot{\theta}_m = L\frac{di}{dt} + iR,\ \tau_m = k_t i, \tag{3}$$

where k_t and k_b are motor torque and back-electromotive constants, respectively. L and R are motor inductance and resistance, respectively, and θ_m denotes motor output angle. From the gearbox ratio n and applied load torque τ_1 to the rotor shaft, we obtain

$$\tau_1 = \tau_m - J_m\ddot{\theta}_m - b_m\dot{\theta}_m, \tag{4}$$

where J_m is the motor moment of inertia and b_m the viscous friction coefficient of the motor bearing. From Fig. 3, let θ_2 and τ_d denote the gearbox output angle and torque, respectively. We then obtain $\theta_2 = \frac{\theta_1}{n}$, $\theta_m = \theta_1$, and $\tau_2 = n\tau_1$. We further denote the stiffness and damping coefficients of the transmission system as k_c and b_c, respectively. The applied torque at the knee joint is then obtained as

$$\tau_d = b_c(\dot{\theta}_2 - \dot{\theta}_k) + k_c(\theta_2 - \theta_k), \tag{5}$$

where $\theta_k = \theta_t - \theta_s$ is the knee rotation angle, θ_t and θ_s are the thigh and shank angles, respectively; see Fig. 1(c). The equation of motion of the knee joint is described as

$$J_h\ddot{\theta}_k = \tau_h + \tau_d = \tau_h + b_c(\dot{\theta}_2 - \dot{\theta}_k) + k_c(\theta_2 - \theta_k) \tag{6}$$

where τ_h is the human applied torque at the knee joint estimated by the synergy model in real time and J_h is the total mass moment of inertia around the knee joint.

Authorized licensed use limited to: City College of New York. Downloaded on May 21,2021 at 18:47:40 UTC from IEEE Xplore. Restrictions apply.

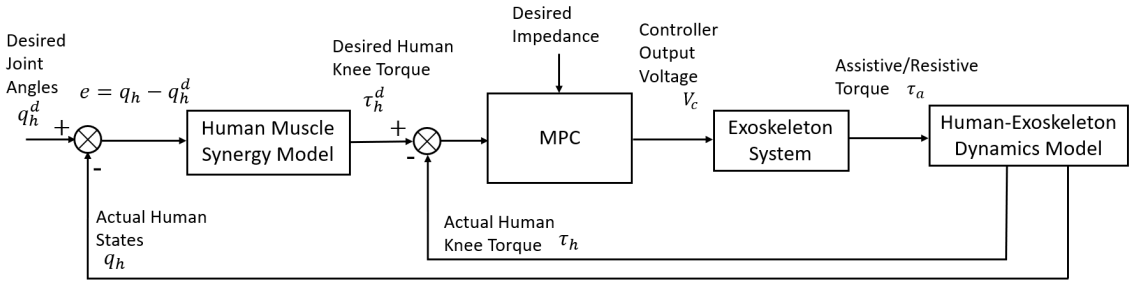

Fig. 2. Schematic flow of the proposed wearable knee device control design.

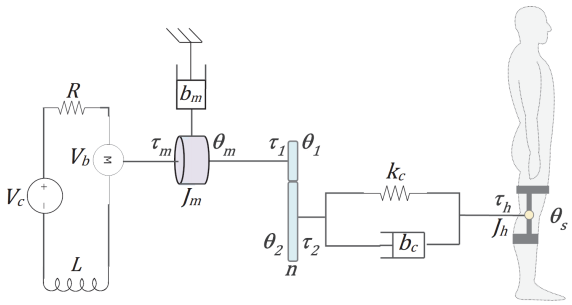

Fig. 3. The schematic of the dynamic model of the human-exoskeleton interactions.

Assuming $L = 0$ in (3) results in $i = \frac{V_c - k_b \dot{\theta}_m}{R}$ and a reduction in the order of the dynamic model. Defining the state variable $\boldsymbol{q} = [\theta_m \ \dot{\theta}_m \ \theta_k \ \dot{\theta}_k]^T$ and output $\boldsymbol{y} = [\theta_k \ \dot{\theta}_k \ \tau_d]^T$, the state space model of the human-device interaction is obtained as

$$\dot{\boldsymbol{q}} = \boldsymbol{A}\boldsymbol{q} + \boldsymbol{B}_v V_c + \boldsymbol{B}_\tau \tau_h, \ \ \boldsymbol{y} = \boldsymbol{C}\boldsymbol{q} \tag{7}$$

where

$$\boldsymbol{A} = \begin{bmatrix} 0 & 1 & 0 & 0 \\ \frac{-k_t k_b n^2 - k_c R}{n^2 J_m R} & \frac{-b_m n^2 - b_c}{n^2 J_m} & \frac{k_c}{n J_m} & \frac{b_c}{n J_m} \\ 0 & 0 & 0 & 1 \\ \frac{k_c}{n J_h} & \frac{b_c}{n J_h} & \frac{-k_c}{J_h} & \frac{-b_c}{J_h} \end{bmatrix},$$

$$\boldsymbol{B}_v = \begin{bmatrix} 0 \\ \frac{k_t}{J_m R} \\ 0 \\ 0 \end{bmatrix}, \ \boldsymbol{B}_\tau = \begin{bmatrix} 0 \\ 0 \\ 0 \\ \frac{1}{J_h} \end{bmatrix}, \ \boldsymbol{C} = \begin{bmatrix} 0 & 0 & 1 & 0 \\ 0 & 0 & 0 & 1 \\ \frac{k_c}{n} & \frac{b_c}{n} & -k_c & -b_c \end{bmatrix}.$$

III. Assist-As-Needed Control Design

Fig. 2 illustrates the assist-as-needed control design. The main control components include the human muscle synergy-based torque prediction, physical human-assistive device interactions, and the MPC system.

Although the QDD motor provides a low back-drivability feature, it is desired that it exhibit a specific response external disturbance and excitation. We define the desired impedance model as

$$J_d \ddot{\theta}_m + b_d^m \dot{\theta}_m - b_d^s \dot{\theta}_k + k_d^m \theta_m - k_d^s \theta_k = \tau_c, \tag{8}$$

where J_d, b_d^m, b_d^s, k_d^m and k_d^s are the desired inertia, viscous and stiffness coefficients and τ_c is the new control input to stimulate the system. We design a controller for (7) to regulate its behavior as by the desired impedance model (8). From the second equation of (7), we obtain

$$\ddot{\theta}_m = f(\boldsymbol{q}) + \frac{k_t}{J_m R} V_c, \tag{9}$$

where $f(\boldsymbol{q}) = -\left(\frac{k_t k_b n^2 + k_c R}{n^2 J_m R}\right)\theta_m - \left(\frac{b_m n^2 + b_c}{n^2 J_m}\right)\dot{\theta}_m + \frac{k_c}{n J_m}\theta_s + \frac{b_c}{n J_m}\dot{\theta}_s$. Using (8), we obtain

$$V_c = -\frac{J_m R}{k_t}\Big[f(\boldsymbol{q}) - \frac{1}{J_d}\big(b_d^m \dot{\theta}_m - b_d^s \dot{\theta}_k + k_d^m \theta_m - k_d^s \theta_k - \tau_c\big)\Big].$$

We consider an MPC design for control input torque τ_c. Using the discrete-time model the cost function $J(k)$ for the MPC design at the kth step is described as

$$J(k) = \sum_{i=k}^{k+H} \left[w_a(\tau_d^d(i) - \tau_d(i))^2 + w_c \Delta\tau_c(i)^2\right], \tag{10}$$

where $w_a, w_c > 0$ are positive weights of the output torque difference $e_\tau(i) = \tau_d^d(i) - \tau_d(i)$ and control torque difference $\Delta\tau_c(i) = \tau_c(i+1) - \tau_c(i)$, $i = k, \ldots, k+H$, $H \in \mathbb{N}$ is the control horizon. τ_d^d is the desired reference torque for the robotic device. The cost function is subject to the constraints

$$\theta_k^{\min} \le \theta_k \le \theta_k^{\max}, \ \dot{\theta}_k^{\min} \le \dot{\theta}_k \le \dot{\theta}_k^{\max}, \ \tau_d^{\min} \le \tau_d \le \tau_d^{\max},$$

where $\tau_d^{\min}$ ($\tau_d^{\max}$), $\theta_k^{\min}$ ($\theta_k^{\max}$), and $\dot{\theta}_k^{\min}$ ($\dot{\theta}_k^{\max}$) are the lower (upper) bounds of the knee joint torque, joint angle and joint angular velocity, respectively.

To obtain the desired reference torque τ_d^d, we define the normal knee torque as τ_h^d as

$$\tau_h^d = \tau_h + \tau_d^d, \tag{11}$$

where τ_h^d is estimated by the muscle synergy model. We use $\tau_d^d = \alpha \tau_h^d$, $0 \le \alpha \le 1$, to select an assistive torque τ_d^d. Intuitively it follows that under this design, we assume that $\tau_h = (1 - \alpha)\tau_h^d$ and it would reduce the human energy expenses. In the simulation experiments, we vary the parameter α to demonstrate the device's effectiveness.

IV. HIL-Simulation and Results

Table I lists the parameter values of the human-exoskeleton system. Most of these values are taken from the physical systems and experiments in [15]. Using the Matlab API, we simulate the assistive device that is attached to subject's thigh and shank in the OpenSim model.

Authorized licensed use limited to: City College of New York. Downloaded on May 21,2021 at 18:47:40 UTC from IEEE Xplore. Restrictions apply.

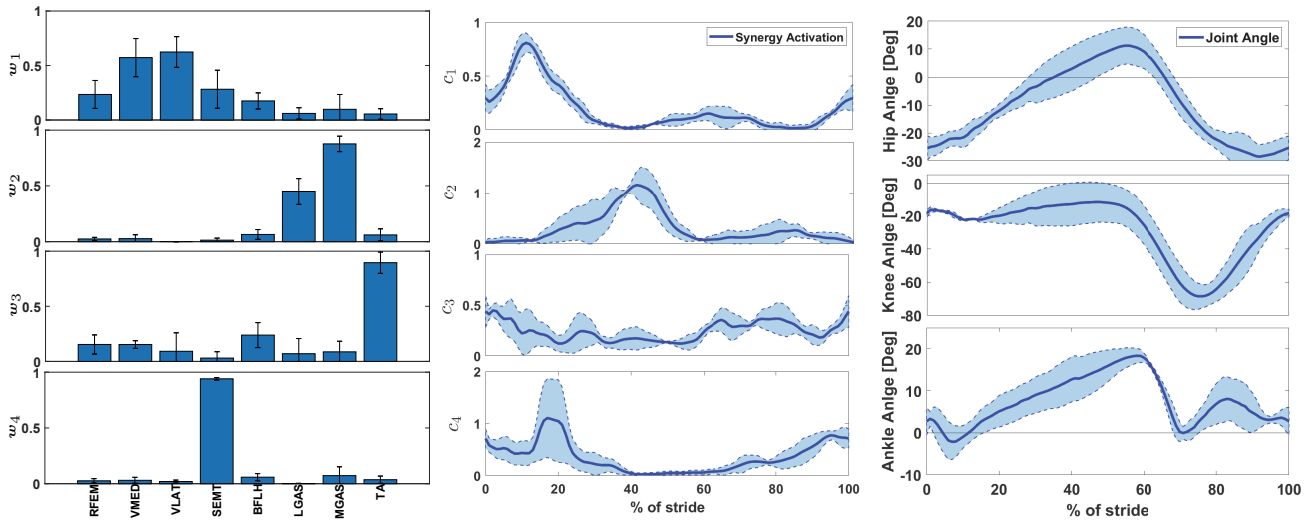

(a) (b) (c)

Fig. 4. Experimental results for multiple subjects. (a) Muscle synergy pattern for normal walking. Human lower-limb synergies. Each synergy contains eight muscles: RFEM, VMED, VLAT, SEMT, BFLH, LGAS, MGAS, and TA. (b) Human muscle synergy activation from EMG-based reconstruction method. (c) Averaged joint angles of the right knee for multiple subjects. The top figure displays the hip angle profile, the middle figure presents the knee profile and the bottom illustrates the ankle profile.

TABLE I

TYPICAL PARAMETERS OF THE HUMAN-EXOSKELETON SYSTEM

Parameter	Value	Unit
Rated Voltage	42	V
Rated Current	7.5	A
Rated Torque	2.165	Nm
Motor Resistance	0.58	Ω
Motor Inductance	0.21	mH
Motor Friction Coefficient	0.08	$Nm \cdot s/rad$
Torque Constant	0.2886	Nm/A
Motor Inertia	895	$g \cdot cm^2$
Gear Ratio	8 : 1	-
Transmission Stiffness	500	Nm/rad
Transmission Damping	0.01	$Nm \cdot s/rad$

We briefly explain the relationship of muscle synergies and muscle activation. Four synergies are selected for the human lower-limb motion as they can reliably reproduce more than 90 % of EMG signals from experiments. Fig. 4(a) shows the synergy patterns as a histogram and the variances of each muscle excitation level. The four synergies used here are related to the knee and ankle movements. The first five muscles in the synergy are crucial for knee extension and retraction (Synergies 1 and 4) while the remaining are linked to the ankle movement (Synergies 2 and 3). From these results, we observe that different subjects indeed experience a similar synergy pattern during normal walking.

As shown in the Fig. 4(b), three synergy activation levels $c_i(t)$, $i = 1, 2, 4$, achieve their peak values at different time moments. For example, synergy $\boldsymbol{w}_1$ mostly contributes at the start of the cycle and is related to stride initiation. In Fig. 4(b), the blue shaded area is one standard deviation from average synergy activation of all the subjects. Each synergy pattern is associated with a base synergy force vector

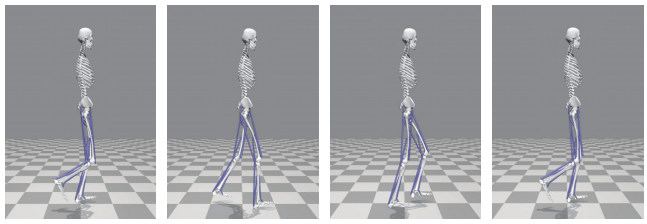

(a) $t = 0.5$ s (b) $t = 1$ s (c) $t = 1.5$ s (d) $t = 2$ s

Fig. 5. Snapshot of unassisted walking of a subject from left to right at $t = 0.5, 1, 1.5, 2$ s.

$\boldsymbol{A}_F$ and we predict joint torques by using the relationship in (2). Fig. 4(c) shows the hip, knee and ankle joint angles over stride during normal walking. The stride starts with a right foot heel strike and ends at the next heel strike. The blue curve shows the average angle profile in our normal walking experiments. The blue shaded area shows one standard deviation from average angles.

A total of 4 subjects with an average mass of 80.75 kg were selected to acquire EMG, GRF and motion data using a Vicon Motion Capture system. Force sensors are placed on the heel and instep of each shoe. Fig. 5 shows the snapshots of the OpenSim results at $t = 0.5$, 1, 1.5 and 2 s. We present the results with assistive torque ratio $\alpha = 0\%, 25\%$ and 50%. A torque ratio $\alpha = 0$ serves as the reference, i.e., normal walking without any assistance. The estimated knee torque is derived from the neural network predictor that was trained using a combination of EMG readings, knee, hip and ankle angle data. Fig. 6 shows the torque prediction result. It is clear that the predicted torque matches with the ground truth closely.

Fig. 7 shows the human applied torques at knee, ankle and hip joints under various α values. These results indicate that the knee assistive robot reduces the human applied torque

Authorized licensed use limited to: City College of New York. Downloaded on May 21,2021 at 18:47:40 UTC from IEEE Xplore. Restrictions apply.

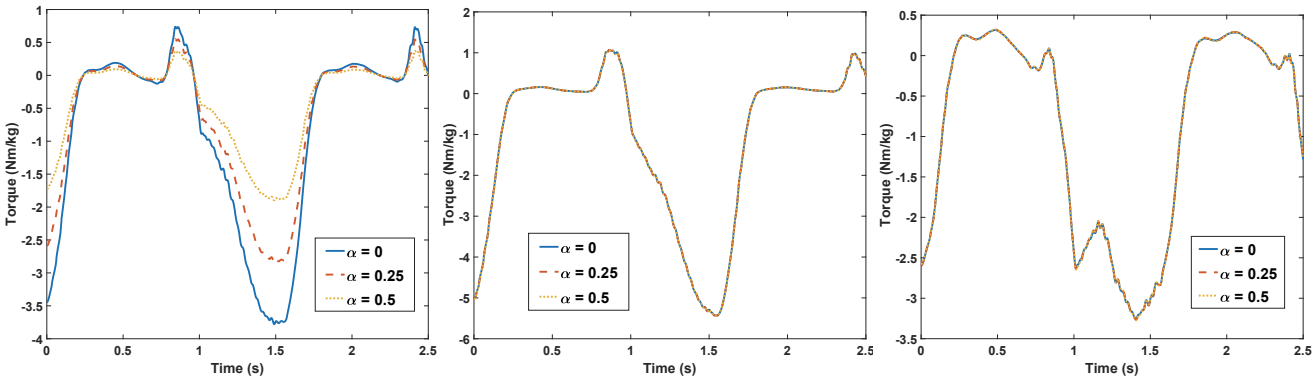

(a) (b) (c)

Fig. 7. Human joint torques under different levels of assistance $\alpha = 0, 0.25, 0.5$. (a) Knee torque. (b) Ankle torque. (c) Hip torque.

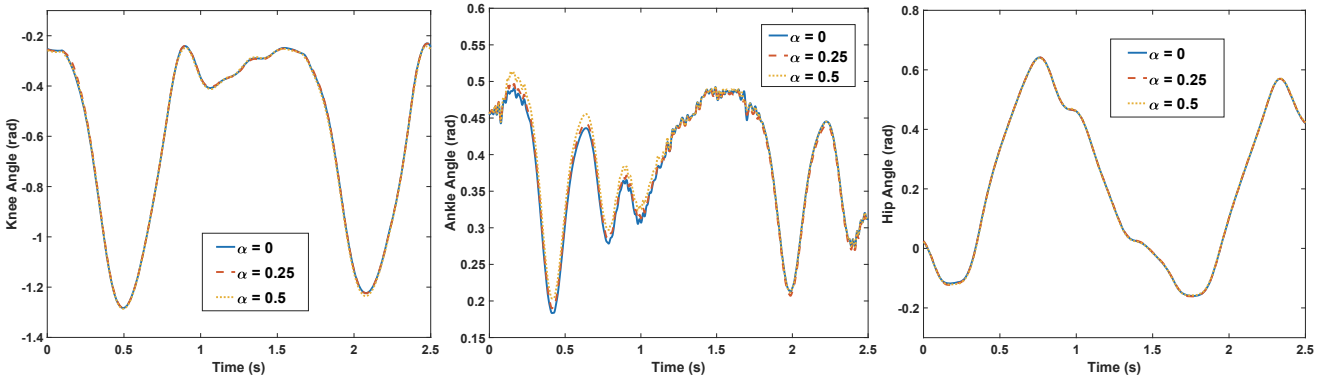

(a) (b) (c)

Fig. 8. Human joint angles under different levels of assistance $\alpha = 0, 0.25, 0.5$. (a) Knee angle. (b) Ankle angle. (c) Hip angle.

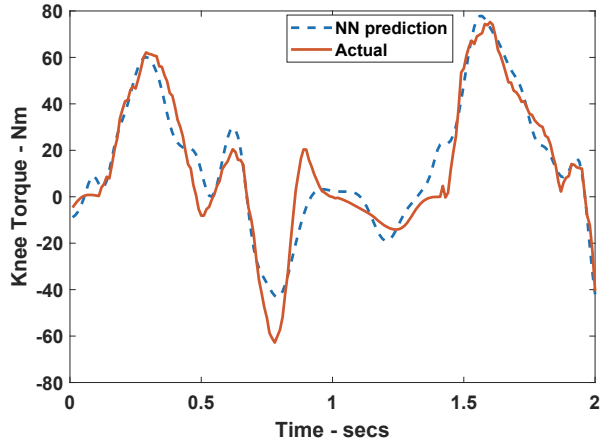

Fig. 6. Knee torque prediction performance.

(Fig. 7(a)). The ankle and hip joint torques are unchanged as α varies; see Figs. 7(b) and 7(c). Figs. 8(a)-8(c) show the corresponding knee, ankle and hip joint angles under $\alpha = 0, 0.25, 5$, respectively. It is clear that even with varying knee torques, all joint angles are the same under different levels of knee joint assistance.

Fig. 9 shows the synergy activation levels c_i, $i = 1, 2, 3, 4$ under various assistance levels. Notice that the synergy level c_1 has a large variation under different α values, while no significant changes are observed in synergy activation levels c_2, c_3 and c_4. This is due to the fact that only synergy $\boldsymbol{w}_1$ has an impact on knee torque and other three synergies have almost no significant effects. With a large α value, a reduced synergy activation level c_1 (for $\boldsymbol{w}_1$) is observed. Indeed, the synergy activation c_1 is decreased by 13.4% and 61.3% for $\alpha = 0.25$ and 0.5, respectively.

The metabolic cost is an indication of the energy consumed by a subject and we expect an inverse relationship with the assistive torque. Note that the first synergy $\boldsymbol{w}_1$ is associated with the MGAS and BFLH muscles and synergy $\boldsymbol{w}_1$ mainly contributes to knee torque generation. Figs. 10(a) and 10(b) show the instantaneous and accumulated metabolic costs of the MGAS muscle. Similarly, Figs. 10(c) and 10(d) demonstrate the instantaneous and accumulated metabolic costs of the BFLH muscle. All of these results have confirmed that under a large assistance provided by the knee exoskeleton, the human energy expenses are reduced.

V. Conclusion

We presented an assist-as-needed interface control of a QDD knee exoskeleton for human walking. The QDD actuation provided high-torque, high-backdrivability and high-bandwidth and it is attractive for wearable human assistive devices. An MPC design was presented to integrate the design with predicted human motion intention and joint

Authorized licensed use limited to: City College of New York. Downloaded on May 21,2021 at 18:47:40 UTC from IEEE Xplore. Restrictions apply.

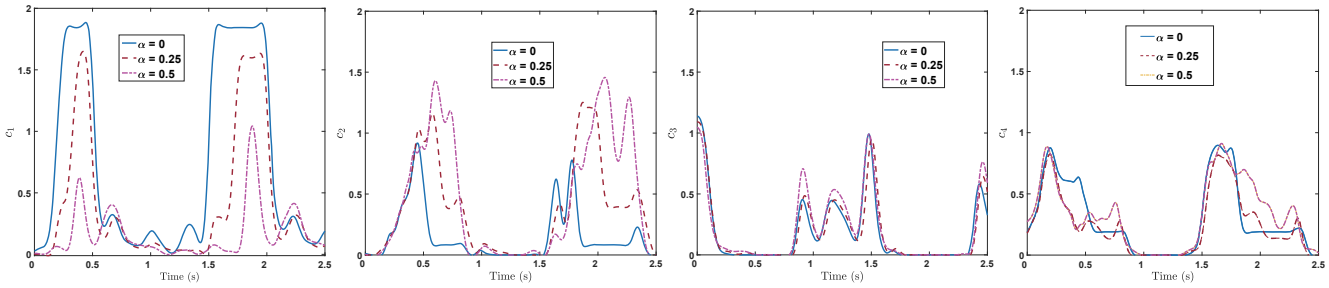

(a) (b) (c) (d)

Fig. 9. Synergy activation level under various assistance levels $\alpha = 0, 0.25, 0.5$. (a) c_1. (b) c_2. (c) c_3. (d) c_4.

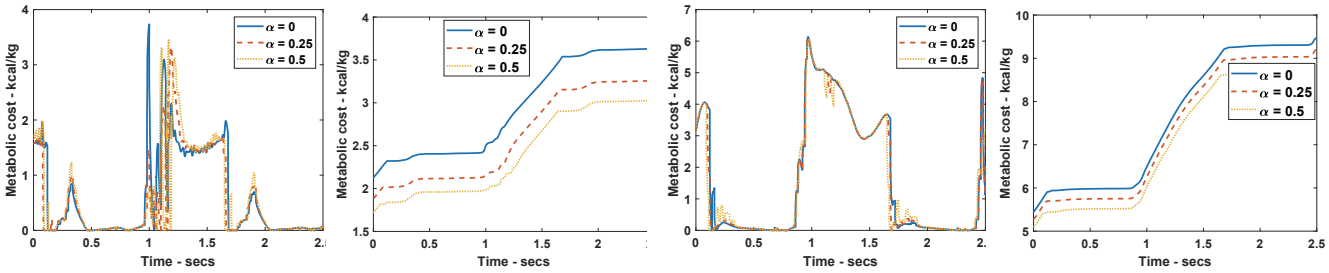

(a) (b) (c) (d)

Fig. 10. Metabolic cost of two muscles under various assistance levels $\alpha = 0, 0.25, 0.5$. (a) Instantaneous profile of the MGAS muscle. (b) Accumulated profile of the MGAS muscle. (c) Instantaneous profile of the BFLH muscle. (d) Accumulated profile of the BFLH muscle.

torque. We used experimental data from normal walking and simulated the control design in OpenSim. The results from the simulations indicated that under the assistance by the knee exoskeleton, the human applied torque was reduced. Our future work involves the testing and validation of our design in this paper. Exploring how to select values of α its relationship to the reduction of metabolic cost and synergies is a part of our future.

REFERENCES

[1] M. Trkov, K. Chen, J. Yi, and T. Liu, "Inertial sensor-based slip detection in human walking," *IEEE Trans. Automat. Sci. Eng.*, vol. 17, no. 1, pp. 348–360, 2020.

[2] M. Trkov, K. Chen, and J. Yi, "Bipedal model and extended hybrid zero dynamics of human walking with foot slips," *ASME J. Computat. Nonlinear Dyn.*, vol. 14, no. 10, 2019, article 101002.

[3] C. R. Reid, P. M. Bush, W. Karwowski, and S. K. Durrani, "Occupational postural activity and lower extremity discomfort: A review," *Int. J. Ind. Ergonom.*, vol. 40, pp. 247–256, 2010.

[4] J. Zhang, P. Fiers, K. A. Witte, R. W. Jackson, K. L. Poggensee, C. G. Atkeson, and S. H. Collins, "Human-in-the-loop optimization of exoskeleton assistance during walking," *Science*, vol. 356, pp. 1280–1284, 2017.

[5] M. Trkov, S. Wu, K. Chen, J. Yi, T. Liu, and Q. Zhao, "Design and characterization of a robotic knee assistive device (ROKAD) for slip-induced fall prevention during walking," in *Proc. IFAC World Congress*, Toulouse, France, 2017, pp. 10 218–10 223.

[6] T. Yan, M. Cempini, C. M. Oddo, and N. Vitiello, "Review of assistive strategies in powered lower-limb orthoses and exoskeletons," *Robot. Auton. Syst.*, vol. 64, pp. 120–136, 2015.

[7] A. J. Young and D. P. Ferris, "State of the art and future directions for lower limb robotic exoskeletons," *IEEE Trans. Neural Syst. Rehab. Eng.*, vol. 25, no. 2, pp. 171–182, 2017.

[8] Y. Ma, X. Wu, J. Yi, C. Wang, and C. Chen, "A review on human-exoskeleton coordination towards lower limb robotic exoskeleton systems," *Int. J. Robot. Automat.*, vol. 34, no. 4, pp. 431–451, 2019.

[9] J. S. Sulzer, R. A. Roiz, M. A. Peshkin, and J. L. Patton, "A highly backdrivable, lightweight knee actuator for investigating gait in stroke," *IEEE Trans. Robotics*, vol. 25, no. 3, pp. 539–548, 2009.

[10] M. K. Shepherd and E. J. Rouse, "Design and validation of a torque-controllable knee exoskeleton for sit-to-stand assistance," *IEEE/ASME Trans. Mechatronics*, vol. 22, no. 4, pp. 1695–1704, 2017.

[11] Z. F. Lerner, D. L. Damiano, and T. C. Bulea, "A lower-extremity exoskeleton improves knee extension in children with crouch gait from cerebral palsy," *Sci. Transl. Med.*, vol. 9, no. 404, p. eaam9145, 2017.

[12] S. Sridar and P. H. Nguyen and M. Zhu and Q. P. Lam and P. Polygerinos, "Development of a soft-inflatable exosuit for knee rehabilitation," in *Proc. IEEE/RSJ Int. Conf. Intell. Robot. Syst.*, Vancouver, BC, 2017, pp. 3722–3727.

[13] Y. Ding, M. Kim, S. Kuindersma, and C. J. Walsh, "Human-in-the-loop optimization of hip assistance with a soft exosuit during walking," *Sci. Robot.*, vol. 3, no. 15, p. eaar5438, 2018.

[14] S. Yu, T.-H. Huang, D. Wang, B. Lynn, D. Sayd, V. Silivanov, Y. S. Park, Y. Tian, and H. Su, "Design and control of a high-torque and highly backdrivable hybrid soft exoskeleton for knee injury prevention during squatting," *IEEE Robot. Automat. Lett.*, vol. 4, no. 4, pp. 4579–4586, 2019.

[15] S. Yu, T.-H. Huang, X. Yang, C. Jiao, J. Yang, H. Hu, S. Zhang, Y. Chen, J. Yi, and H. Su, "Quasi-direct drive actuation for a lightweight hip exoskeleton with high backdrivability and high bandwidth," *IEEE/ASME Trans. Mechatronics*, 2020, in press.

[16] A. S. McIntosh, K. T. Beatty, L. N. Dwan, and D. R. Vickers, "Gait dynamics on an inclined walkway," *J. Biomech.*, vol. 39, no. 13, pp. 2491–2502, 2006.

[17] P. M. Wensing, A. Wang, S. Seok, D. Otten, J. Lang, and S. Kim, "Proprioceptive actuator design in the MIT cheetah: Impact mitigation and high-bandwidth physical interaction for dynamic legged robots," vol. 33, no. 3, pp. 509–522, 2017.

[18] S. A. Chvatal and L. H. Ting, "Common muscle synergies for balance and walking," *Front. Comput. Neurosci.*, vol. 7, 2013, article 48.

[19] A. Sawers, Y.-P. Pai, T. Bhatt, and L. H. Ting, "Neuromuscular responses differ between slip-induced falls and recoveries in older adults," *J. Neurophysiol.*, vol. 117, pp. 509–522, 2017.

[20] S. Chen, J. Yi, and T. Liu, "Strength capacity estimation of human upper limb in human-robot interactions with muscle synergy models," in *Proc. IEEE/ASME Int. Conf. Adv. Intelli. Mechatronics*, Auckland, New Zealand, 2018, pp. 1051–1056.

[21] ——, "Muscle synergy-based control of human-manipulator interactions," in *Proc. IEEE/ASME Int. Conf. Adv. Intelli. Mechatronics*, Boston, MA, 2020.

[22] http://opensim.stanford.edu/.

Authorized licensed use limited to: City College of New York. Downloaded on May 21,2021 at 18:47:40 UTC from IEEE Xplore. Restrictions apply.